Journal of
Computational and Theoretical Nanoscience
Vol. 15, 542–550, 2018

RESEARCH ARTICLE

Analysis of Functionally Graded Quantum-Dot Systems with Graded Lattice Mismatch Strain

Peter L. Bishay[1,*], Jan Sladek[2], Ernian Pan[3], and Vladimir Sladek[2]

[1] *College of Engineering and Computer Science, California State University, Northridge, 91330, USA*
[2] *Institute of Construction and Architecture, Slovak Academy of Sciences, 84503 Bratislava, Slovakia*
[3] *Department of Civil Engineering, University of Akron, Akron, OH 44325-3905, USA*

The production methodology of alloyed quantum-dot (QD) structures introduced a new design degree of freedom for QD arrays which is the grading of the material composition in the QD growth direction. This enables QDs of same size to generate different colors when exposed to blue light based on the grading of each QD. The grading of the material composition affects the material properties as well as the lattice mismatch strain between the QDs and the host matrix. Previous studies modeled graded QDs by just considering graded lattice mismatch strain while the material properties were kept uniform. Because these previous studies were seeking analytical solutions, including a graded material property model would have complicated the solutions. In this paper, a fully-coupled thermo-electro-mechanical finite element model of a cylindrical functionally graded QD (FGQD) in a host piezoelectric matrix is developed with both graded material properties and graded lattice mismatch strain. Different cases are considered corresponding to separately increasing and decreasing the strength of the lattice mismatch strain and the material properties in the QD thickness direction. The grading function is expressed using the power law that enables fractional exponents. The results show the effect of grading on the electromechanical quantities and demonstrate the flexibility that grading can add to the design of QD arrays. This work contributes to the development of quantum dots with "grading-dependent color" rather than the traditional "size-dependent color." The model can be easily extended to other cases such as different shapes of QDs, addition of wetting layer, and any applied thermo-electro-mechanical loads.

Keywords: Low-Dimensional Semiconductors Nanostructures, Eigenstrain, Piezoelectricity, Finite Element.

1. INTRODUCTION

As the world's most efficient light emitting technology, quantum-dots (QDs) represent a truly enabling nanotechnology and offer revolutionary advantages in their wide range of applications such as solid state lighting, power efficient LEDs for superior performance in displays and photovoltaics, solar cells, quantum computing and medical imaging.[1] Quantum dots are tiny particles or nanocrystals of a semiconducting material with diameters in the range of 2–10 nanometers that display unique electronic properties, intermediate between those of bulk semiconductors and discrete molecules that are partially the result of the unusually high surface-to-volume ratios for these particles. The most apparent result of this is fluorescence, wherein the nanocrystals can produce distinctive colors determined by the size of the particles. Due to their small size, the electrons in QDs are confined in a small space (quantum box), and when the radius of the semiconductor nanocrystal is smaller than the exciton Bohr radius (the average distance between the electron in the conduction band and the hole it leaves behind in the valence band), there is quantization of the energy levels. Generally, as the size of the crystal decreases, the difference in energy between the highest valence band and the lowest conduction band increases. More energy is then needed to excite the dot, and concurrently, more energy is released when the crystal returns to its ground state, resulting in a color shift from red to blue in the emitted light. As a result of this phenomenon, QDs can be tuned during manufacturing to emit any color of light from the same material simply by changing the dot size.

*Author to whom correspondence should be addressed.

 1546-1955/2018/15/542/009 doi:10.1166/jctn.2018.7120

Low-dimensional semiconductor nanostructures (LDSNs), like QDs, are normally embedded in a host material with different material properties and lattice parameters,[2] hence they are strained structures. Strain in both the QD and the host matrix relax elastically to accommodate the lattice mismatch and thus admit a new state of stress. Because of the spatially confined motion of electrons in QDs, the electronic structure and the consequent optoelectronic properties are functions of the lattice-mismatch induced strain. Since most semiconductor materials are piezoelectric in nature,[1] strain and piezoelectric effects are being used as tuning parameters for the optical response of LDSNs in band gap engineering. On the other hand, thermal effects coupled with electrical and mechanical fields in LDSNs have also become important, thus temperature became another tuning parameter.

Several analytical and computational studies have analyzed the electromechanical fields in QD systems (See Ref. [1] and the references therein). For example, Patil and Melnik[1] presented a finite element model to study the coupled thermo-electro-mechanical effects in uniform QDs under thermal loadings. Their studies assumed uniform material properties and eigenstrain (or mismatch strain). On the other hand, alloyed QDs (e.g., $In_xGa_{1-x}As$ and $CdTe_xSe_{1-x}$) have attracted much interest recently because the behavior of any electronic device made of these alloyed QDs is strongly affected by their enriched but non-uniform composition.[3–7] The production methodology adopted for manufacturing alloyed QDs enables the composition of the QD to be graded, hence affecting the material properties as well as the induced mismatch strain between the QD and the carrier matrix.[8,9] The possibility of tuning a particular composition profile via alloying represents another degree of freedom in the design of self-assembled heteroepitaxial structures.[10]

Exact closed-form solutions were developed for QDs of different shapes (spherical, cylindrical, ellipsoidal, pyramidal, and arbitrarily shaped polygonal) with graded eigenstrain in piezoelectric matrix (See Refs. [11–13] and the references therein). For example, exact closed-form solutions were derived for an arbitrarily shaped polygonal inclusion with any order of polynomial eigenstrains in an anisotropic magneto-electro-elastic full plane.[11] Solutions of linearly[12] and quadratically[13] graded eigenstrain in an anisotropic piezoelectric half plane were also developed. All the developed analytical models relied on two main assumptions:

(1) The grading function of the eigenstrains is polynomial. This is based on the fact proved by Eshelby that if the eigenstrain inside an ellipsoidal inclusion is in the form of a polynomial in Cartesian coordinates, the induced strain field in the inclusion is also characterized by a polynomial of the same order.[14] This assumption facilitates obtaining closed-form solutions. However, it should be noted that the eigenstrains may not be explicitly given in a polynomial form.[15]

(2) The graded composition of the QD material affects only the eigenstrains, while the material properties can be assumed constant. Grading the material properties would complicate the analytical models and render finding a closed-form solution very difficult if not impossible.

This paper presents a fully coupled finite element model of a cylindrical functionally graded QD (FGQD) system with functionally graded material properties and graded lattice mismatch strain in a host piezoelectric matrix. The variations of the material properties and lattice mismatch strain are applied in the thickness direction and using the power law (fractional exponents). The effects of the material property ratio, mismatch strain ratio and the power law index on the mechanical and electrical fields of the functionally graded QD system are analyzed for four cases considering the possibilities of increasing or decreasing the intensity of the mismatch strain and the material properties in the thickness direction. The rest of the paper is organized as follows: Section 2 presents the governing equations and boundary conditions, Section 3 introduces the grading functions used to describe the effective material properties and lattice mismatch strain. Section 4 describes the FE model. Section 5 presents the results, and final conclusions are in Section 6.

2. GOVERNING EQUATIONS AND BOUNDARY CONDITIONS

The linear governing equations of steady state thermo-electro-elasticity for a structure occupying volume Ω, are the balance of linear momentum, Gauss's law for electrostatics, and the stationary heat conduction equation:

$$\sigma_{ij,j} + f_i = 0; \quad D_{i,i} + q = 0; \quad h_{i,i} - k = 0 \qquad (1)$$

where σ_{ij}, D_i, h_i are the components of the stress tensor, electric displacement vector, and heat flux vector, and f_i, q and k are the mechanical body force vector, electric charge and heat source in Ω, respectively.

Gradient equations in the mechanical, electrical and thermal domains are expressed as:

$$\varepsilon_{kl} = \frac{1}{2}(u_{k,l} + u_{l,k}); \quad E_k = -\phi_{,k}; \quad Q_k = -T_{,k} \qquad (2)$$

where, $\varepsilon_{kl}, E_k, Q_k, u_k, \phi$ and T are the components of the strain tensor, electric field vector, temperature gradient vector, mechanical displacement vector, electric potential and temperature change from the reference temperature T_0, respectively. Assuming the problem domain is under thermal equilibrium, temperature change becomes

spatially independent and only the first two equations in Eqs. (1) and (2) need to be solved.

The constitutive relations relating thermo-electro-mechanical quantities are expressed as,

$$\begin{aligned} \sigma_{ij} &= c_{ijkl}\varepsilon_{kl} + e_{ijk}E_k - \beta_{ij}T; \\ D_i &= e_{ikl}\varepsilon_{kl} + \in_{ik} E_k + p_i T + P_i^{sp}; \\ S &= \beta_{ij}\varepsilon_{ij} + p_i E_i + \alpha_T T \end{aligned} \tag{3}$$

where, c_{ijkl}, e_{ijk} and $\in_{ik}$ are the elastic moduli, piezoelectric coefficients, and dielectric constants, respectively, while P_i^{sp}, p_i and β_{ij} are spontaneous polarization vector, thermoelectric and thermomechanical coupling constants, respectively. In cylindrical coordinates, the strain tensor components in Eq. (2) can be expressed, taking into account the lattice mismatch, as:

$$\begin{aligned} \varepsilon_{rr} &= \frac{\partial u_r}{\partial r} - \varepsilon_a^*; \quad \varepsilon_{zz} = \frac{\partial u_z}{\partial z} - \varepsilon_c^*; \\ \varepsilon_{\theta\theta} &= \frac{u_r}{r} - \varepsilon_a^*; \quad \varepsilon_{rz} = \frac{1}{2}\left(\frac{\partial u_r}{\partial z} + \frac{\partial u_z}{\partial r}\right) \end{aligned} \tag{4}$$

with $\varepsilon_a^* = (a_m - a_{\mathrm{QD}})/a_{\mathrm{QD}}$ and $\varepsilon_c^* = (c_m - c_{\mathrm{QD}})/c_{\mathrm{QD}}$ inside the QD. ε_a^*, ε_c^* are the local intrinsic strains (lattice mismatch) along the a- and c-directions, respectively, while a_m, c_m and a_{QD}, c_{QD} are the lattice constants of the matrix and the QD, respectively. The directions a and c correspond to the shorter and longer dimensions of the unit cell of the Wurtzite (WZ) crystal, respectively. As the substrate is relatively large compared to the QD, we follow common practice to neglect lattice mismatch strain inside the matrix.[1, 16–19]

The material properties for WZ structures as well as the geometry and boundary conditions in this study are axisymmetric (no angular dependence), hence all electric and mechanical fields are axisymmetric as well, and the problem is reduced from 3D to 2D in the plane involving the axis of cylindrical symmetry. The linearly independent elastic constants and piezoelectric constants in a crystal with WZ symmetry are then given as

$$\begin{gathered} c_{11} = c_{1111}, \quad c_{12} = c_{1122}, \quad c_{13} = c_{1133}, \\ c_{33} = c_{3333}, \quad c_{44} = c_{2323}, \\ c_{21} = c_{2121} = (c_{11} - c_{12})/2, \\ e_{31} = e_{311}, \quad e_{33} = e_{333}, \quad e_{15} = e_{113} \\ \beta_1 = \beta_{11}, \quad \beta_3 = \beta_{33}, \quad \in_1 = \in_{11}, \quad \in_3 = \in_{33} \end{gathered} \tag{5}$$

Figure 1 (left) shows the geometric details of the cylindrical QD system considered in this study, where the QD has a radius of $b = 4$ nm and a height of $h_{\mathrm{QD}} = 4$ nm, while the height of the carrier matrix is $L = 30$ nm and its diameter $D = 2W = 120$ nm. The geometry and dimensions considered here are based on experimental results (reported in Ref. [20]). In this study, we choose GaN/AlN QD system, which can be analyzed as representative of III–V group semiconductors. The material properties of this QD system are given in Ref. [1]. The values of the lattice mismatch strain for GaN/AlN QD system are: $\varepsilon_a^* = -2.47\%$ and $\varepsilon_c^* = -4.07\%$.

Mechanical rollers and electric ground boundary conditions are imposed along the top and bottom faces of the system (see Fig. 1 (left)), the right face is traction free and electrically isolated, while symmetry boundary conditions ($u_r = 0$, $\partial u_z/\partial r = 0$, $\partial\phi/\partial r = 0$) are applied along z-axis. Temperature can range from 0 to 1000 K to cover most thermoelectric applications of interest.

3. GRADING FUNCTION FOR MATERIAL PROPERTIES AND LATTICE MISMATCH INDUCED STRAIN IN FGQDs

A functionally graded material (FGM) is a continuous medium defined by the variation in the volume fractions of its constituents. The power-law function, exponential function, or sigmoid function have been used to describe the volume fractions of an FGM. A power law type definition for the volume fraction across the thickness direction (z) can be given as:[21]

$$f(z) = \left(0.5 + \frac{z}{h_{\mathrm{QD}}}\right)^n \quad \text{where } z \in \left[-\frac{h_{\mathrm{QD}}}{2}, \frac{h_{\mathrm{QD}}}{2}\right] \tag{6}$$

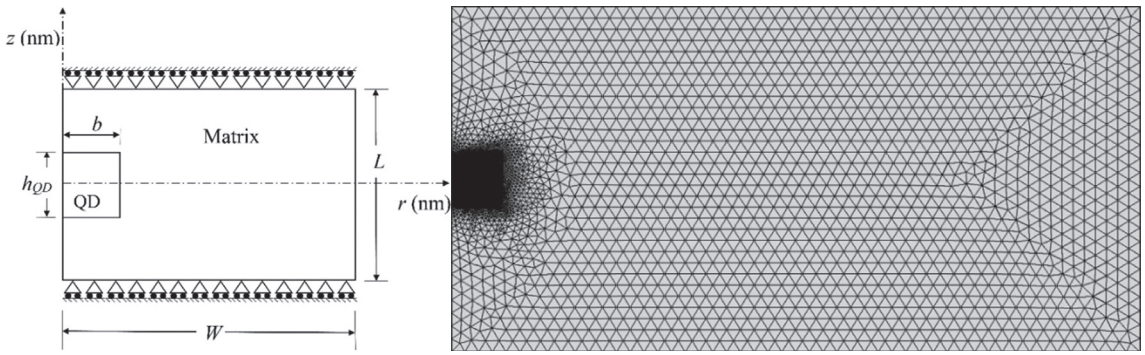

Fig. 1. (left) Geometry and coordinate system in (r, z) plane for cylindrical QD system (axisymmetric model), (right) COMSOL finite element mesh.

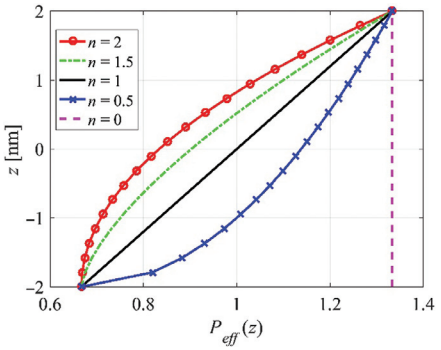

Fig. 2. The effective material property $P_{\text{eff}}(z)$ in the QD.

where h_{QD} is the height of the QD and n is the power law index. When $n = 1$, the variation in volume fraction is linear in the thickness direction. If n is less than 1, the nonlinear grading function goes quicker to the value at the top of the QD, while if n is larger than 1, the grading function goes slower to the value at the top of the QD as we move vertically upwards. Based on the volume fraction definition and law of mixtures, the effective properties of an FGM in the thickness direction can be expressed as:

$$P_{\text{eff}}(z) = P[1+\gamma(2f(z)-1)];$$
$$\gamma = \frac{P_u - P_l}{P_u + P_l}; \quad P = \frac{P_u + P_l}{2} \tag{7}$$

where $P_{\text{eff}}(z)$ is the effective material property of the FGM; subscripts u and l denote, respectively, the upper and lower surface property of the FGM solid. $P_u = P_{\text{eff}}(h_{\text{QD}}/2) = P(1+\gamma)$ and $P_l = P_{\text{eff}}(-h_{\text{QD}}/2) = P(1-\gamma)$. When $n = 0$, $P_{\text{eff}} = P_u = P(1+\gamma)$ and when $n = \infty$, $P_{\text{eff}} = P_l = P(1-\gamma)$ inside the QD. Figure 2 shows $P_{\text{eff}}(z)$ for the case of $h_{\text{QD}} = 4$ nm, $P = 1$, $\gamma = 1/3$ and different values of n.

In this study, we assume that grading the material in the thickness direction will affect all material properties in Eq. (5) in the same fashion. Hence,

$$\frac{(c_{ij})_l}{(c_{ij})_u} = \frac{(e_{ij})_l}{(e_{ij})_u} = \frac{(\epsilon_i)_l}{(\epsilon_i)_u} = \frac{(\beta_i)_l}{(\beta_i)_u}$$
$$= \frac{(p_i)_l}{(p_i)_u} = \frac{(P_i^{sp})_l}{(P_i^{sp})_u} = \frac{1-\gamma}{1+\gamma} \tag{8}$$

If $\gamma < 0$, then the magnitude of the material properties decreases in the thickness direction, while if $\gamma > 0$, the magnitude increases as the QD grows.

The effective mismatch strains of a FGQD can be expressed similarly as:

$$\varepsilon^*_{a_{\text{eff}}}(z) = \varepsilon^*_a[1+\rho(2f(z)-1)];$$
$$\varepsilon^*_{c_{\text{eff}}}(z) = \varepsilon^*_c[1+\rho(2f(z)-1)];$$

$$\rho = \frac{\varepsilon^*_{a_u} - \varepsilon^*_{a_l}}{\varepsilon^*_{a_u} + \varepsilon^*_{a_l}} = \frac{\varepsilon^*_{c_u} - \varepsilon^*_{c_l}}{\varepsilon^*_{c_u} + \varepsilon^*_{c_l}}; \tag{9}$$
$$\varepsilon^*_a = \frac{\varepsilon^*_{a_u} + \varepsilon^*_{a_l}}{2}; \quad \varepsilon^*_c = \frac{\varepsilon^*_{c_u} + \varepsilon^*_{c_l}}{2}$$

where $\varepsilon^*_{a_u} = \varepsilon^*_{a_{\text{eff}}}(h_{\text{QD}}/2) = \varepsilon^*_a(1+\rho)$, $\varepsilon^*_{a_l} = \varepsilon^*_{a_{\text{eff}}}(-h_{\text{QD}}/2) = \varepsilon^*_a(1-\rho)$ and similarly for $\varepsilon^*_{c_u}$ and $\varepsilon^*_{c_l}$. It is important to note that ρ could be different from γ. This allows considering four possibilities for increasing or decreasing mismatch strain with increasing or decreasing magnitude of the material properties. The same power law function $f(z)$ in Eq. (6) is used for the two considered types of grading. It should be emphasized that as n increases, larger portion of the QD will have values of material properties and mismatch strain closer to the values at the bottom of the QD.

4. FINITE ELEMENT MODELING

Using the governing equations described in Section 2, an FEM model was developed in COMSOL Multiphysics.[22] The *Piezoelectric Devices* (pzd) user interface under the *Structural Mechanics* branch in COMSOL, combining *Solid Mechanics* and *Electrostatics* for modeling piezoelectric devices, is used in these simulations. Initial stress ($\boldsymbol{\sigma}_0$), initial strain ($\boldsymbol{\varepsilon}_0$), and remanent electric displacement ($\mathbf{D}_r$) can be defined in the stress-charge formulation of the constitutive relation for piezoelectric materials:

$$\boldsymbol{\sigma} - \boldsymbol{\sigma}_0 = \mathbf{c}_E(\boldsymbol{\varepsilon} - \boldsymbol{\varepsilon}_0) - \mathbf{e}^T\mathbf{E}; \quad \mathbf{D} - \mathbf{D}_r = \mathbf{e}(\boldsymbol{\varepsilon} - \boldsymbol{\varepsilon}_0) + \boldsymbol{\varepsilon}_S\mathbf{E} \tag{10}$$

where $\boldsymbol{\varepsilon}$ is the strain, $\boldsymbol{\sigma}$ is the stress tensor written in vector form, $\mathbf{E}$ is the electric field, and $\mathbf{D}$ is the electric displacement field vectors. The material properties $\mathbf{c}_E$, $\mathbf{e}$, and $\boldsymbol{\varepsilon}_S$ correspond to the material stiffness tensor, piezoelectric coupling tensor (written in matrix form), and the electric permittivity matrix.

Two grading functions are defined in the FEM model, $f_1(z)$ for material grading and $f_2(z)$ for eigenstrain grading:

$$f_1(z) = 1+\gamma(2f(z)-1); \quad f_2(z) = 1+\rho(2f(z)-1) \tag{11}$$

where $f(z)$, γ and ρ are defined in Eqs. (6), (7), and (9), respectively.

The initial stress and strain tensors, written in matrix form, in the FG GaN QD take the form:

$$\boldsymbol{\sigma}_0 = \begin{pmatrix} -\beta_1 & 0 & 0 \\ 0 & -\beta_1 & 0 \\ 0 & 0 & -\beta_3 \end{pmatrix} f_1(z);$$
$$\boldsymbol{\varepsilon}_0 = \begin{pmatrix} -\varepsilon^*_a & 0 & 0 \\ 0 & -\varepsilon^*_a & 0 \\ 0 & 0 & -\varepsilon^*_c \end{pmatrix} f_2(z) \tag{12}$$

In the AlN carrier matrix, the initial strain is assumed zero, while the initial stress takes the same form of $\boldsymbol{\sigma}_0$ in Eq. (12) without $f_1(z)$.

The remnant electric displacement field vector $\mathbf{D}_r$ accounts for the pyroelectric effect and the spontaneous polarization, and is defined as:

$$\mathbf{D}_r = \begin{pmatrix} 0 \\ 0 \\ p_3 T + P^{sp} \end{pmatrix} f_1(z) \tag{13}$$

where β_1, β_3, p_3 and P^{sp} in Eqs. (12) and (13) take the values of the corresponding material in each domain. The grading function $f_1(z)$ is also multiplied by the material matrices in Eq. (10): $c_E \Rightarrow c_E f_1(z)$, $e \Rightarrow e f_1(z)$, $\varepsilon_S \Rightarrow \varepsilon_S f_1(z)$ in the FGQD domain.

It was found that a convergent solution with smooth distribution of electromechanical quantities at $r = 0$ can be achieved with "Extra Fine" mesh in the matrix domain (with maximum element size, m, of 1.2 nm) that is refined as we approach the domain of the QD which has $m = 0.1$. The selected mesh which is composed of 9,365 higher order triangular elements is shown in Figure 1 (right).

5. RESULTS

The developed FEM model was first validated for the case of uniform material properties and eigenstrain by comparison with the published results in Refs. [1, 17, and 23]. Excellent agreement was found in all cases. In this section, we present the effect of material and eigenstrain grading on the electro-mechanical behavior of GaN QD in AlN matrix. This system is selected because of the relatively prominent piezoelectric nature of Wurtzite materials compared to the Zincblende materials. Subsection 5.1 presents the effect of the material property ratio (γ), Subsection 5.2 presents the effect of the mismatch strain ratio (ρ), Subsection 5.3 combines both effects of γ and ρ, and Subsection 5.4 shows the effect of the grading function exponent (n) on the electromechanical quantities in the FGQD and the host matrix.

An important point to note is that for band-gap calculations, the mismatch strain is subtracted from the actual compatible elastic strain. As a result, while in the solid mechanics community, the compatible elastic strain is normally expressed and plotted, the QD research community often illustrates the subtracted strain. This can potentially cause confusion and care must be exercised in interpreting results from the solid mechanics literature.[1] In the strain plots in this section we plot ε_{rr} and ε_{zz} as defined in Eq. (4).

5.1. Effect of Material Property Ratio γ

In this study we demonstrate the effect of grading the material properties of the QD in the thickness direction using linear grading function ($n = 1$) and with uniform eigenstrain in the QD ($\rho = 0$). The temperature is kept constant at 300 K. Figure 3 shows the electromechanical variables along the axis of symmetry ($r = 0$) of the cylindrical QD for three cases of material property ratio

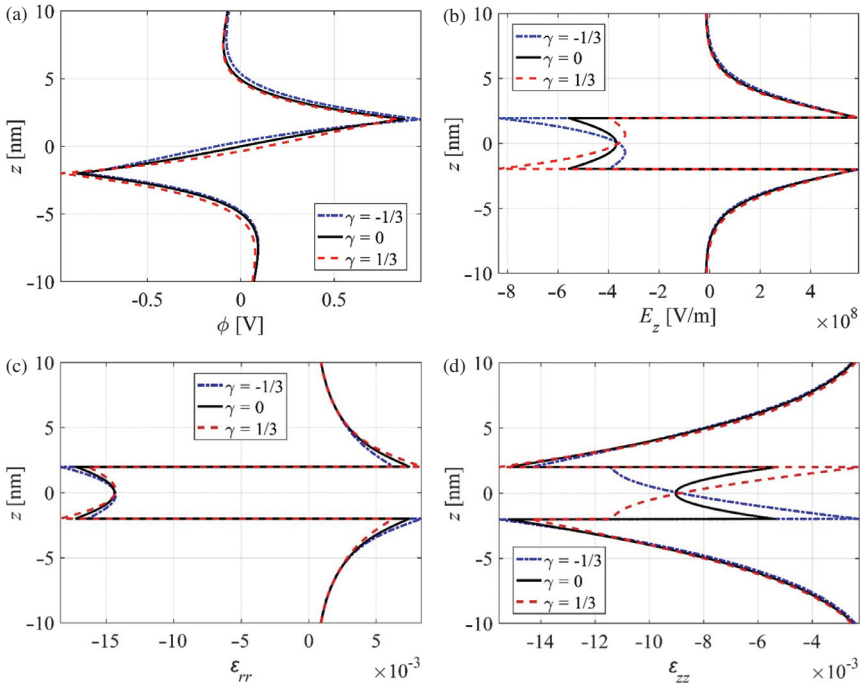

Fig. 3. Effect of material property ratio γ on the electromechanical quantities of cylindrical GaN/AlN FGQD system with $\rho = 0$, $n = 1$, and constant temperature of 300 K: (a) electric potential ϕ, (b) electric field E_z, (c) strain ε_{rr}, and (d) strain ε_{zz}.

γ. $\gamma = 0$ corresponds to no grading, while $\gamma = 1/3$ corresponds to increasing magnitude of all material properties in the z-direction (or magnitude of all material properties at the bottom of the QD is half that at the top of the QD), and $\gamma = -1/3$ corresponds to decreasing magnitude of all material properties in the z-direction (or magnitude of all material properties at the bottom of the QD is double that at the top of the QD).

It can be seen that as γ increases, the electric potential difference across the thickness of the QD remains constant, the magnitude of vertical electric field E_z at the bottom of the QD increases while that at the top decreases. The magnitude of the compressive ε_{rr} at the bottom of the QD increases while that of the tensile ε_{rr} in the host matrix below the QD decreases. Finally the magnitude of compressive ε_{zz} at the bottom of the QD highly increases and gets much larger than that at the top of the QD, while that of the compressive ε_{zz} in the host matrix below the QD decreases.

5.2. Effect of the Mismatch Strain Ratio ρ

Now we demonstrate the effect of grading the mismatch strain (eigenstrain) on the electromechanical quantities in the QD system considering linear grading function ($n = 1$) while keeping uniform material properties in the QD ($\gamma = 0$). Again three cases are considered: $\rho = 0$ corresponds to uniform (ungraded) mismatch strain, while $\rho = 1/3$ indicates that the magnitude of the mismatch strain at the bottom of the QD is half that at the top, and $\rho = -1/3$ indicates that the magnitude of mismatch strain at the bottom of the QD is double that at the top. Figure 4 shows the electromechanical variables along the axis of symmetry of a cylindrical QD for the three cases of lattice mismatch strain ratio ρ. It can be observed that as ρ increases, the electric potential difference along the QD remains constant, the magnitudes of E_z and ε_{rr} decrease at the base of the QD and in the host matrix below the QD. However, the magnitude of the compressive ε_{zz} highly increases at the base and decreases at the top of the QD. As ρ decreases, the jump in ε_{zz} that happens through the base of the QD is significantly reduced because of the reduction of ε_{zz} in the host matrix and its increase in the QD, while the jump at the top of the QD gets larger.

It is very interesting to note that the effect of ρ is qualitatively opposite to that of γ on the z-component of electric displacement (E_z), and the radial component of strain (ε_{rr}) inside the QD, while both ρ and γ have qualitatively similar effects on the z-component of the strain (ε_{zz}) inside the QD, and ε_{rr} in the host matrix. It is also interesting to note that ρ has much stronger effect on ε_{rr} than γ, while both ρ and γ have quantitatively similar effects on ε_{zz}.

5.3. Effect of Varying the Material Property Ratio and the Mismatch Strain Ratio Simultaneously

After understanding the effects of varying γ and ρ separately on the QD system, we allow both γ and ρ to vary

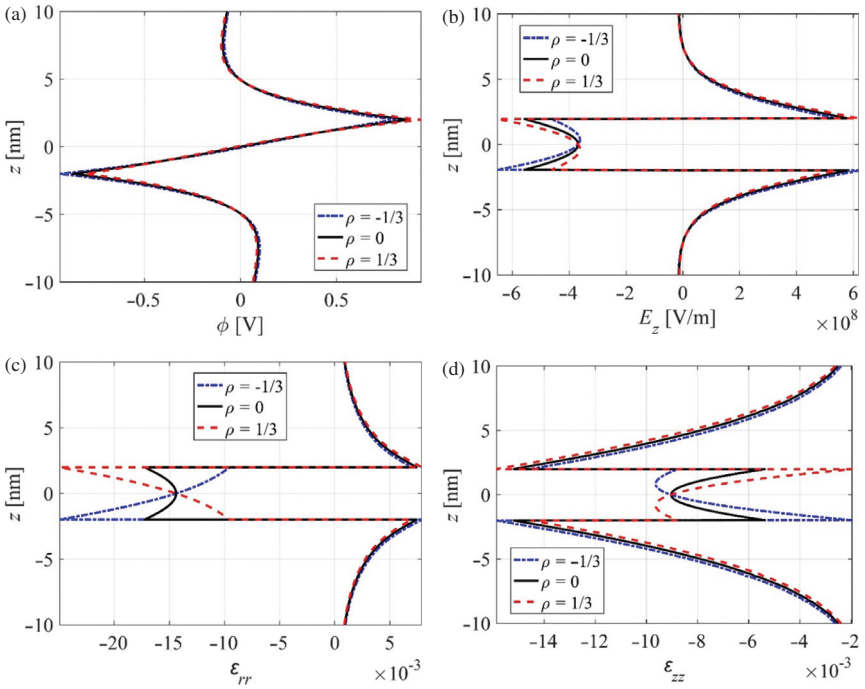

Fig. 4. Effect of initial lattice mismatch strain ratio ρ on the electromechanical quantities of cylindrical GaN/AlN FGQD system with $\gamma = 0, n = 1$, and constant temperature of 300 K: (a) electric potential ϕ, (b) electric field E_z, (c) strain ε_{rr}, and (d) strain ε_{zz}.

RESEARCH ARTICLE

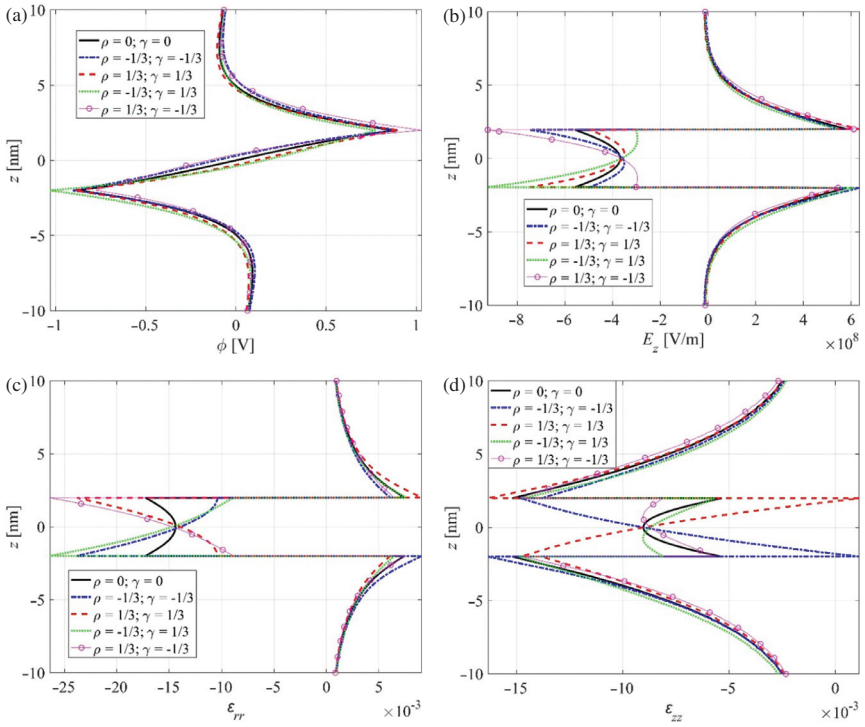

Fig. 5. Effect of varying the material property ratio γ and the mismatch strain ratio ρ on the electromechanical quantities of cylindrical GaN/AlN FGQD system with $n = 1$ and constant temperature of 300 K: (a) electric potential ϕ, (b) electric field E_z, (c) strain ε_{rr}, and (d) strain ε_{zz}.

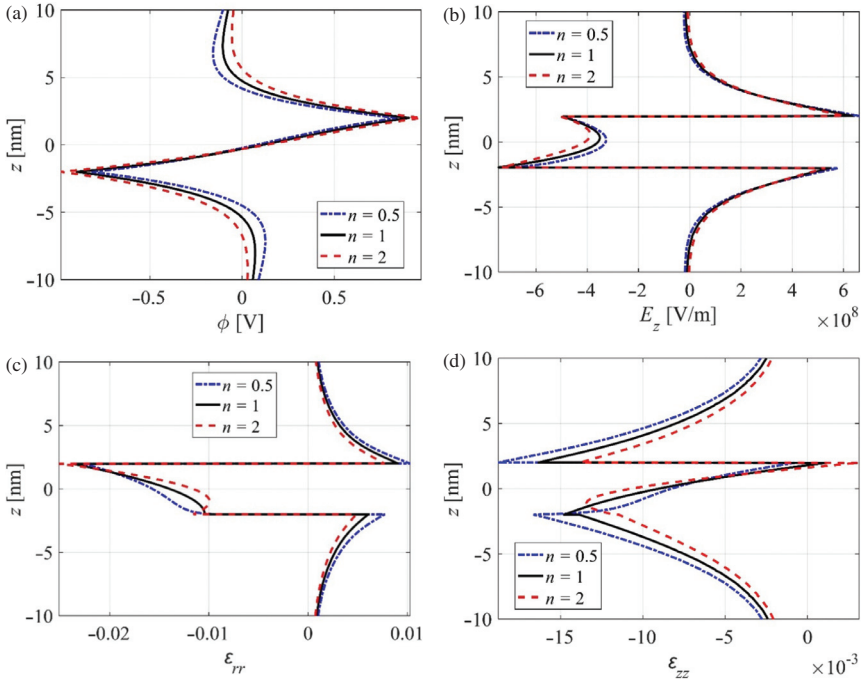

Fig. 6. Effect of varying the power law index on the electromechanical quantities of cylindrical GaN/AlN FGQD system at a constant temperature of 300 K, $\rho = 1/3$ and $\gamma = 1/3$ (a) electric potential ϕ, (b) electric field E_z, (c) strain ε_{rr}, and (d) strain ε_{zz}.

simultaneously in this study which provides more realistic cases because grading the composition of the QD in the growth direction is expected to affect the material properties as well as the induced lattice mismatch strain. We consider four cases here corresponding to increasing or decreasing the mismatch strain and the magnitude of material properties in the thickness direction. Figure 5 shows these four cases in addition to the ungraded case ($\gamma = \rho = 0$) to facilitate the comparison. It can be seen that although the distribution of ϕ changes, the electric potential difference across the height of the QD remains constant. The case of ($\rho = -1/3,\ \gamma = 1/3$) results in the maximum magnitude of E_z and ε_{rr} at the base of the QD, while the opposite case ($\rho = 1/3, \gamma = -1/3$) results in the maximum magnitude of E_z and ε_{rr} at the top surface of the QD. This behavior is expected based on the observations drawn in the previous two subsections. The case of ($\rho = 1/3, \gamma = 1/3$) results in the maximum magnitude of ε_{zz} at the base of the QD, while the opposite case ($\rho = -1/3, \gamma = -1/3$) maximizes ε_{zz} at the top of the QD. These results would provide important guidance to device designers. For example if the design requirements are to achieve maximum magnitude of E_z at the top surface of the QD, the composition of the grown QD should be designed such that the magnitude of the material properties decreases in the thickness direction while the lattice mismatch strain increases.

5.4. Effect of the Power Law Index

Figure 6 shows the effect of the power law index (n) on the electromechanical quantities of the FG GaN/AlN QD system for the case of increasing the magnitudes of the material properties and the mismatch strain ($\rho = 1/3, \gamma = 1/3$) in the thickness direction at a constant temperature of 300 K. Three cases are considered for n: 0.5, 1, 2. It can be observed that as n increases, the electric potential difference along the height of the QD increases, the magnitude of E_z in the QD increases, the magnitudes of ε_{rr} and ε_{zz} decrease in the host matrix around the QD, and their curvatures inside the QD change. The electric potential difference across the height of the QD, that was shown to be unaffected by variations in the grading ratios ρ and γ, is directly proportional to the power law index n.

6. SUMMARY AND CONCLUSIONS

In this study, a fully coupled thermo-electro-mechanical finite-element model for functionally-graded quantum dot in a piezoelectric matrix was developed. Grading of the material properties as well as the lattice mismatch strain were considered, and the effects of different cases of grading on the electromechanical quantities in the QD system were studied. The power law was used to express the nonlinear grading functions in the FGQD, and the effect of the power law index was also presented.

It is the first time that grading in both material properties and lattice mismatch strain is considered and accordingly the results in this paper are believed to be more accurate than the previous analytical models that used graded mismatch strain with uniform material properties. This work contributes to the development of quantum dots with "grading-dependent color" rather than the traditional "size-dependent color." Grading is now a new tuning parameter to be added to the other design variables of QD arrays such as shape, size, mismatch strain, piezoelectric coupling and temperature, giving the designers larger design space for next-generation quantum dot structures and devices.

The developed model can be extended to other cases such as different shapes of QDs in 2D (dome, truncated cone, etc.) or 3D (cube, polygon, etc.), addition of wetting layer, and any applied thermo-electro-mechanical loads.

Acknowledgment: The first author acknowledges the support of California State University, Northridge. The second and fourth authors gratefully acknowledge the supports of the Slovak Science and Technology Assistance Agency registered under number APVV-14-0216 and the Slovak Grant Agency VEGA-2/0046/16.

References

1. S. Patil and R. V. N. Melnik, *Nanotechnology* 20, 12 (**2009**).
2. R. Maranganti and P. Sharma, Handbook of Theoretical and Computational Nanotechnology, edited by M. Rieth and W. Schommers, American Scientific Publisher, CA (**2005**), Vol. 1, pp. 1–44.
3. C. Lang, D. Nguyen-Manh, and D. J. H. Cockayne, *J. Appl. Phys.* 94, 7067 (**2003**).
4. C. Lang, D. J. H. Cockayne, and D. Nguyen-Manh, *Phys. Rev. B* 72, 155328 (**2005**).
5. H. L. Duan, B. L. Karihaloo, J. Wang, and X. Yi, *Phys. Rev. B* 74, 195328 (**2006**).
6. R. E. Bailey and S. M. Nie, *Journal of American Chemical Society* 125, 7100 (**2003**).
7. J. Tersoff, *Phys. Rev. Lett.* 81, 3183 (**1998**).
8. H. L. Duan, B. L. Karibaloo, J. Wang, and X. Yi, *Nanotechnology* 17, 3380 (**2006**).
9. G. H. Nie, L. Guo, C. K. Chan, and F. G. Shin, *International Journal of Solids and Structures* 44, 3575 (**2007**).
10. A. Malachias, S. Kycia, G. Medeiros-Ribeiro, R. Magalhaes-Paniago, T. I. Kamins, and R. S. Williams, *Phys. Rev. Lett.* 91, 176101 (**2003**).
11. Y. G. Lee, W. N. Zou, and E. Pan, *Proceedings of the Royal Society of London A* 471, 20140827 (**2015**).
12. Q. D. Chen, K. Y. Xu, and E. Pan, *International Journal of Solids and Structures* 51, 53 (**2014**).
13. Y. M. Yue, K. Y. Xu, Q. D. Chen, and E. Pan, *Acta Mechanica* 226, 2365 (**2015**).
14. J. D. Eshelby, *Proceedings of the Royal Society of London A, Mathematical and Physical Sciences* 241, 376 (**1957**).
15. P. Sharma and R. Sharma, *Journal of Applied Mechanics* 70, 418 (**2003**).
16. R. Maranganti and P. Sharma, *J. Comput. Theor. Nanosci.* 4, 715 (**2003**).

17. B. Lassen, M. Willatzen, D. Barettin, R. V. N. Melnik, and L. C. Voon, *Journal of Physics: Conference Series* 107, 10701 **(2008)**.

18. A. D. Andreev and E. P. O'Reilly, *Phys. Rev. B* 62, 15851 **(2000)**.

19. A. D. Andreev and E. P. O'Reilly, *Physica E: Low-Dimensional Systems and Nanostructures* 10, 553 **(2001)**.

20. M. Arley, J. L. Rouviere, F. Widmann, B. Daudin, G. Feuillet, and H. Mariette, *Appl. Phys. Lett.* 74, 3287 **(1999)**.

21. S. H. Chi and Y. L. Chung, *International Journal of Solids and Structures* 43, 3657 **(2006)**.

22. COMSOL is the developer of COMSOL Multiphysics software, an interactive environment for modeling and simulating scientific and engineering problems (Web link: www.comsol.com).

23. D. Barettin, B. Lassen, and M. Willatzen, *Journal of Physics: Conference Series* 107, 012001 **(2008)**.

24. A. D. Andreev and E. P. O'Reilly, *Nanotechnology* 11, 256 **(2000)**.

25. S. Lee, O. L. Lazarenkova, P. Allmen, F. Oyafuso, and G. Klimeck, *Physical Review B* 70, 125307 **(2004)**.

Received: 31 August 2017. Accepted: 10 September 2017.